THE JOURNAL OF PHYSICAL CHEMISTRY C
A JOURNAL OF THE AMERICAN CHEMICAL SOCIETY

pubs.acs.org/JPCC
Article

The Effect of Weakly Adsorbed Cations on the Helmholtz Capacitance of Metal−Water Interfaces

Fabiola Domínguez-Flores,* Axel Groß, and Wolfgang Schmickler

Cite This: https://doi.org/10.1021/acs.jpcc.5c08002
Read Online

ACCESS | Metrics & More | Article Recommendations

ABSTRACT: The interface between a weakly adsorbed, solvated cation and a metal electrode is investigated by density functional theory using a hybrid implicit-explicit solvation model. The cations remain charged upon adsorption, the counter-charge resides on the metal surface. There is no diffuse double-layer in this system; experimentally this corresponds to adsorption from a low concentration of cations. The change $\Delta\phi$ in electrode potential upon adsorption is determined from the change in the electrostatic potential at large distances from the electrode. The phenomenon of partial charge transfer leads to two separate operational definitions for the charge on the ions: the formal charge ze_0, where z is the valency, and the partial charge remaining after adsorption, which we quantify with the Bader charge. The measurable integral capacitance is determined by ze_0, and for all systems investigated it lies in a range which compares well with experimental data. The divalent ions Ca^{2+} and Mg^{2+} show a substantial partial charge transfer, which enhances the capacitance. In contrast, alkali ions K^+ and Na^+ keep their unit charge. Since there is no diffuse layer, the electrosorption valency equals the negative of the partial charge transfer. Interpreting our results within a simple parallel plate capacitor model allows us to calculate an effective dielectric constant, governed mainly by contributions from the polarizabilities of the metal surface and of the water molecules. Thus, our model provides important insights into the structure of the compact double-layer and its concomitant interactions.

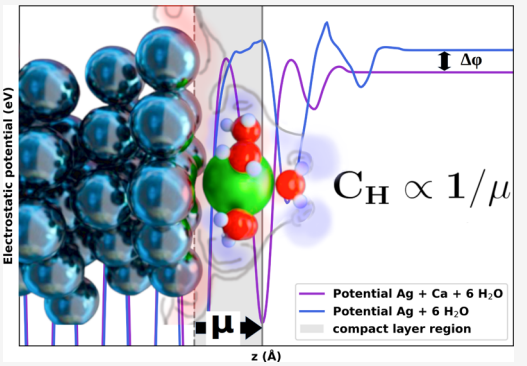

1. INTRODUCTION

The electric double-layer is the heart of an electrochemical system. It is the critical interface where electrochemical reactions happen, and its structure and response to changes in the electrode potential determine its capacitance, i.e. the fundamental relation between electric charge and potential.

Consequently, double-layer theory has been a central research topic for over a century. Yet a truly satisfactory double-layer theory exists only for low electrolyte concentrations and small excess charges: this is the venerable Gouy−Chapman theory[1,2] which treats ions as point charges in a dielectric continuum. Despite extensive efforts to extend these models to a general theory valid at higher electrolyte concentrations such as are used in electrocatalysis (e.g., 0.1 M or higher), the attempts have been essentially futile. At these concentrations, system-specific properties—including the nature, size, and solvation shells of the ions, as well as their interactions with the electrode and its electronic response—become decisive. Nevertheless, continuum approaches neglect key molecular-scale phenomena, such as discrete solvation, ion-specific adsorption, and the structural heterogeneity of interfacial water.

Given the limitations of purely theoretical approaches, researchers have increasingly relied on computational simulations, though these methods face inherent challenges. Classical molecular dynamics (MD) simulations can handle large ensembles and extended time scales but they rely heavily on the accuracy of the force fields used and are constrained in their ability to describe chemical interactions at the electrode−electrolyte interface, particularly the electronic response of the metal surface.[3] Nevertheless, MD has provided important insights into the double-layer structure, especially regarding the solvation shell, reorganization and the potential of mean force as ions approach the electrode.[4−6]

Over the past decades, computational electrochemistry has been dominated by density functional theory (DFT), which has naturally been applied to modeling the electric double-layer (EDL). Ab initio molecular dynamics (AIMD) simulations show how solvation structure, hydrogen bonding, and interfacial water orientation respond to the presence of the electrode.[7] These atomic-scale rearrangements critically determine electric double-layer capacitance, particularly within

Received: November 24, 2025
Revised: January 26, 2026
Accepted: February 2, 2026
Published: February 9, 2026

the compact layer, where ion size effects, specific adsorption, and solvent structure dominate the electrostatic response. Modern computational implementations benefit from schemes that enhance reliability by accounting for the induced electronic response of the metal surface to electrolyte structure.[8] However, despite these advances, AIMD simulations remain computationally too demanding for systematic explorations of electrochemical interfaces.[9] Even with modern computing power, the ensemble sizes that can be practically treated remain too small, and the accessible simulation times too short, to yield a realistic description of the EDL. Moreover, the electrostatic potential, as computed from DFT, is dominated by singularities at the ion cores and does not correspond to the electrostatic potential actually experienced by the extended, nonpoint-like ions.[10,11] While DFT excels at describing chemical interactions, particularly between the electrode surface and adsorbates in close contact—it struggles to capture long-range solvent dynamics and fluctuations that are essential for accurately modeling the capacitance.[12]

Although the measured double-layer capacitance is a property of the entire electrode−electrochemical interface, it also exhibits a local character that is often overlooked. While the potential remains constant within the metal, the interfacial excess charge density, and hence the capacitance, varies with local atomic structure. The adsorption of a single ion constitutes a sizable perturbation, which in our case causes a potential jump of the order of a few volts. Therefore, the derived capacitances are integral rather than differential values; experimentally these can be measured by transient techniques.

Therefore, it is meaningful to study capacitance using the small, well-defined ensembles accessible to DFT. Here, we focus on the Helmholtz layer and examine the role of weakly adsorbed monovalent and divalent cations near well-defined crystalline metal surfaces. In fact, at low ion concentrations of a weakly adsorbed electrolyte the excess charge on the metal is balanced by the charge on the adsorbate, so that the diffuse layer is absent. This has been shown in a number of experimental[13−15] and theoretical works.[16−19] Thus, our model is directly relevant to a certain experimental situation. In addition we note that the capacitance is reduced, if a part of the charge is stored in a diffuse layer. Thus, our results give an upper theoretical limit for the capacitance at a given charge density.

2. METHODS

2.1. Model Systems and Electronic Structure

The present study extends our previously validated DFT approach,[20] preserving all essential computational parameters. We used a mirror-symmetric six-layer 3 × 3 fcc(111) slabs with an identical ion−water assembly on both faces to preserve inversion symmetry on metallic surfaces (Pt, Au, Ag with optimized lattice parameters a = 3.99, 4.21, 4.19 Å respectively). The two central layers were fixed and the outer two layers on each side relaxed. Calculations employed VASP[21,22] with PAW method,[23] RPBE exchange-correlation functional,[24] DFT-D3 dispersion method,[25] a 400 eV plane-wave cutoff, and a Γ-centered 3 × 3 × 1 mesh. Adsorbates (K, Na, Ca, Mg) were placed at hollow sites at 1/9 ML coverage. Long-range solvent interactions were modeled using the VASPsol package[26,27] (dielectric ϵ = 78.4, surface tension τ = 0) and a 20 Å continuum thickness along z-axis. The first hydration shells were constructed with either 6 or 7 water molecules, corresponding to common coordination numbers for aqueous cations. These configurations were initially optimized through short (5−10 ps) DFT-based molecular dynamicsannealing at 300 K, followed by full ionic relaxation. This two-stage protocol ensures both thermally accessible configurations and precise energy minimization of the solvation structures. In the implicit medium there is no vacuum. Reference potentials were taken from flat regions of the continuum solvent on each side of the slab, which are equal by construction. Far away from the surface, the implicit region is just neutral and represents ion-free water (a pure dielectric). We note that our model includes electronic screening from the metal and dielectric response from the solvent, while explicitly excluding diffuse-layer contributions by construction.

2.2. Capacitance and Interfacial Charge

We consider a solvated ion in front of an electrode surface. In our unit cell, this corresponds to 1/9 of coverage. The total charge on the system is zero, so any charge on the ion is compensated by a countercharge on the metal. In what sense can we attribute a capacitance to this arrangement? We use the convention that the potential on the electrode is fixed, so that the potential at large distances from the surface is determined by the work function of the solvated metal. When an ion with charge number z is brought to the surface, a countercharge $-ze_0$ flows onto the electrode, and this is measured as a current. At the same time the potential at large distances changes by an amount $\Delta\phi$. So the natural definition for the capacitance per area A is $C_H = ze_0/(\Delta\phi A)$, where z is the ionic charge, e_0 the elementary charge, and A the interfacial area. We define the formal countercharge density as $\sigma_{formal} \equiv ze_0/A$. Note that C_H depends solely on the total charge transferred, which corresponds to the measurable current in the external circuit. In contrast, the interfacial potential drop $\Delta\phi$ depends critically on how this charge is distributed at the interface.

During adsorption the ion exchanges electrons with the metal surface; this results in a partial charge on the ion which is usually smaller than the charge ze_0 of the ion in the bulk of the solution. Strictly speaking, this partial charge is not well-defined, as it does not correspond to an observable in any extended system. However, different charge partition schemes appear to be qualitatively robust with respect to charge variations after system changes,[28] which is also the main concern in our paper. We have therefore used the widely accepted Bader analysis to derive partial charges, which also help us tounderstand the metaladsorbate interaction. It introduces an image charge on the metal surface, and a corresponding dipole moment $\mu_p = z_p e_0 d$ (where z_p is the partial charge number of the adsorbate, and d is its distance from the image plane of the metal). Note that the formal surface of the metal lies half a lattice spacing in front of the top plane of metal ions, and the effective image plane usually lies about 0.5 Å in front of the formal surface—its exact position is an intrinsic property of the metal and the considered surface plane .[29] While this dipole moment characterizes the ionic bond to the surface, it is not measurable. The charge on the adsorbate induces a screening response at the surface, which opposes the adsorbate dipole. The measurable quantity is the total surface dipole induced by the adsorbate and the response of the surroundings. From elementary electrostatics this is given by $\mu = \Delta\phi\epsilon_0 A$, which has been investigated in our previous publication,[20]. It is related to the capacitances defined above through the relation

$$C_H = ze_0\epsilon_0/\mu \tag{1}$$

Electronic structure calculations have the advantage that they can show system properties that are not directly accessible to experiment, but help greatly in understanding them. In our case, the distribution of the charge and the dielectric response of the interface are of particular interest. Figure 1 shows a typical charge distribution at the interface. The positive charge on the ion induces a net orientation of the surrounding water molecules with their oxygen ends toward the ion. The compensating negative charge on the metal lies in front of the first plane of atoms and is clearly separated from the solvated adsorbate, so the charge density σ on the metal can be evaluated.

We use the induced metal charge, as defined by Bader analysis, as our measure of the operative surface charge. Note that this is always smaller than the formal charge: $|\sigma_{Bader}| < ze_0/A$, thus we define

https://doi.org/10.1021/acs.jpcc.5c08002
J. Phys. Chem. C XXXX, XXX, XXX−XXX

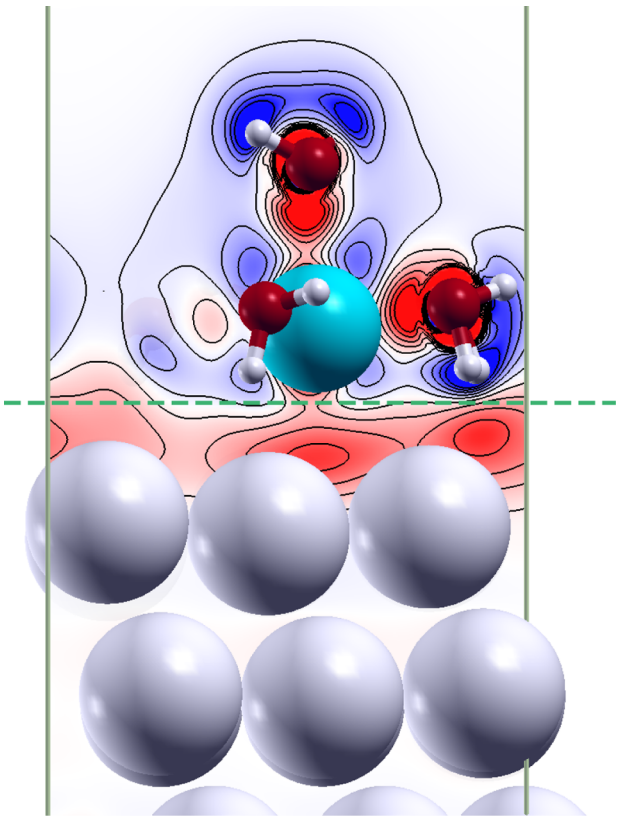

Figure 1. Two-dimensional cross section of the excess charge distribution for a Ca^{2+} with an explicit solvation shell of 6 water molecules adsorbed on Ag(111). Charge-density difference iso-surface at ±0.001 e $Å^{-3}$ (red/blue = accumulation/depletion).

$$C_{op} = \sigma_{Bader}/\Delta\phi \quad (2)$$

We emphasize that C_{op} is not the experimental capacitance, but a useful quantity to characterize the interfacial structure, since it contains the physical charge distribution. The arrangement of charges in our model resembles that of a Helmholtz layer, a venerable concept that is still much used. The corresponding capacitance is often described as that of a parallel plate capacitor with an effective dielectric constant ϵ_{eff}. The latter is ill-defined, but it can be evaluated from our model, with our own C_{op}, through

$$\epsilon_{eff} = C_{op} d/\epsilon_0 \quad (3)$$

For our finite-difference DFT setup at fixed coverage, $\Delta\phi$ is the potential drop between the charged and neutral systems, evaluated from the planar-averaged electrostatic potential in the continuum region and corrected for spurious dipole interactions across the periodic unit-cell boundaries under the implicit-solvent model. This definition automatically includes screening by metal spillover, explicit waters, and the implicit dielectric, as emphasized in.[20] We use two metrics: $C_H = \sigma_{formal}/\Delta\phi$ with $\sigma_{formal} = ze_0/A$, and $C_{op} = \sigma_{Bader}/\Delta\phi = (z\text{-}q_{ion}^{Bader})e_0/A$, where q_{ion}^{Bader} is net Bader charge of the ion (in units of (e_0)), obtained by Bader partitioning of the electron density on the ion. The difference reflects charge partitioning (partial charge transfer), not a different way of computing $\Delta\phi$.

Both capacitances are defined as the ratio of finite differences in charge and potential. As discussed above, they are therefore not differential capacitances as would typically be measured by impedance spectroscopy, but integral capacitances over the interval from 0 to $-\Delta\phi$ with respect to the potential of zero charge (PZC). As can be seen from Table 1, this corresponds to a jump of several volts; such integral capacitances can be measured by a potential step experiment or by cyclic voltammetry.

Table 1. Structural and Electrostatic Properties of Hydrated Ions Near Pt(111), Au(111), and Ag(111) Surfaces[a]

metal	system	(eV)	$\Delta\phi$ (V)	dipole (eÅ)	bader (e)	d_{eff} (Å)	C_H (μFcm^{-2})	C_{op} (μFcm^{-2})	ϵ_{eff} (−)
Pt(111)	Ca^{2+} + $6H_2O$	5.41	2.51	0.86	1.60	1.68	20.59	16.47	3.12
	Ca^{2+} + $7H_2O$	4.67	2.58	0.88	1.68	3.25	20.12	16.82	6.18
	K^+ + $6H_2O$	5.29	1.86	0.64	0.96	3.81	13.83	13.34	7.29
	K^+ + $7H_2O$	5.19	1.65	0.56	0.94	4.84	15.81	14.72	6.33
	Mg^{2+} + $6H_2O$	5.84	2.91	1.00	1.99	1.75	17.76	17.67	3.49
	Mg^{2+} + $7H_2O$	5.18	3.57	1.22	1.96	4.14	14.49	14.20	6.64
	Na^+ + $6H_2O$	5.36	1.82	0.62	0.93	3.58	14.20	13.20	5.34
	Na^+ + $7H_2O$	5.18	1.55	0.53	0.93	3.70	16.67	15.50	6.48
Au(111)	Ca^{2+} + $6H_2O$	4.79	2.47	0.94	1.62	1.57	18.84	15.31	2.71
	Ca^{2+} + $7H_2O$	4.77	3.13	1.19	1.69	2.93	14.88	12.60	4.17
	K^+ + $6H_2O$	4.72	1.72	0.65	0.96	4.82	13.62	13.03	7.09
	K^+ + $7H_2O$	4.72	1.69	0.64	0.95	3.87	13.83	13.12	5.73
	Mg^{2+} + $6H_2O$	4.72	2.46	0.93	1.75	1.69	18.98	16.60	3.17
	Mg^{2+} + $7H_2O$	4.77	3.47	1.32	1.99	5.12	13.45	13.38	7.74
	Na^+ + $6H_2O$	4.67	1.64	0.62	0.94	3.70	14.23	13.38	5.73
	Na^+ + $7H_2O$	4.73	1.66	0.63	0.93	3.79	14.06	13.08	5.46
Ag(111)	Ca^{2+} + $6H_2O$	4.25	2.38	0.91	1.61	1.71	19.46	15.67	3.03
	Ca^{2+} + $7H_2O$	4.22	2.71	1.04	1.69	2.83	17.09	14.44	4.62
	K^+ + $6H_2O$	4.12	1.93	0.74	0.96	4.68	11.97	11.52	6.09
	K^+ + $7H_2O$	3.95	1.52	0.58	0.95	3.70	15.24	14.48	6.05
	Mg^{2+} + $6H_2O$	4.13	2.29	0.88	1.73	1.89	20.23	17.50	3.74
	Mg^{2+} + $7H_2O$	3.98	2.59	0.99	1.99	4.96	17.89	17.80	9.97
	Na^+ + $6H_2O$	4.18	1.72	0.66	0.93	3.18	13.47	12.52	4.50
	Na^+ + $7H_2O$	3.92	1.57	0.60	0.94	3.49	14.75	13.87	5.47

[a] Φ_1: work function (ion-free system).

https://doi.org/10.1021/acs.jpcc.5c08002
J. Phys. Chem. C XXXX, XXX, XXX−XXX

3. RESULTS AND DISCUSSION

Reported Helmholtz capacitances in aqueous electrolytes typically fall in the range ≈10−20 μFcm^{-2} for metallic electrodes. Our results are consistent with classic Hg data and with single-crystal surfaces in dilute, nonspecifically adsorbing electrolytes near the double-layer region,[30,31] see Table 1. The area of our unit cell per adsorbate is of the order of 65 Å^2, so that the formal adsorbed charge densities are ∼24 μC/cm^2 for the monovalent ions, and about twice as much for the divalent ions. Despite these substantial charge densities—corresponding to conditions far from the PZC—the diffuse-layer contribution remains negligible by construction, as the implicit solvent model provides rapid electrostatic screening that confines the potential drop primarily within the compact layer. In our simulations, the per-interface compact-layer capacitances span ≈10−20 μFcm^{-2}, physically reasonable within and at the upper end of the commonly reported experimental range. Note that the compensating charge density on the metal surface carries the opposite sign.

3.1. Hydration Structure Dependence

Let us focus the discussion on the C_H values in the data, which result from the configurations with a more symmetric solvation shell, and comment on the results with an additional H_2O later. First we note that the capacitances for the divalent ions Ca^{2+} and Mg^{2+} are higher than for the monovalent Na^+ and K^+. There are two reasons for this (1) the divalent ions are adsorbed at shorter distances, because their radii are smaller than those of the two alkali ions;[32] in addition they carry higher charges and therefore experience a stronger attraction from their image charges. But note that the effect of the distance is partially offset by the trend in the effective dielectric constant—see the discussion below. (2) Both ions are partially discharged, with the calcium ion losing more charge than the magnesium ion. This reduced charge leads to a smaller $\Delta\phi$ and, consequently, a larger capacitance C_H.

The Ca^{2+} is closer to the surface than Mg^{2+}, and interacts a little stronger with the metal, resulting in a somewhat greater charge transfer. This may seem surprising, since Ca^{2+} has the larger ionic radius of the two. However, its solvation shell is much weaker, according to Marcus[32] Ca^{2+} has a radius of 1.71 Å and a solvation number of 7.2 compared to 2.27 Å and 10.0 for Mg^{2+}. This difference is reflected in the free energies of solvation: 19.03 eV for Mg^{2+} vs 15.65 eV for Ca^{2+}. Consequently, it is less costly in terms of solvation energy to partially discharge Ca^{2+}.

The two alkali ions almost keep their full charge. Their strong solvation shells, small ionization energies, and lower image charge keep them further away from the surface, resulting in smaller capacitances. The larger ionic radius of K^+ compared to Na^+ places it further from the surface resulting in a smaller interfacial capacitance.

We have performed calculations with 6 and with 7 explicit water molecules, so it is of some interest to see what difference the addition of one extra water molecule makes. Because of their smaller charge the interaction of the alkali ions with the extra water is weak, and the results are not systematic—there are too many local minima with similar energies. So we turn to the divalent ions: adding a seventh water molecule increases the distance to the surface for Ca^{2+} and Mg^{2+}. This results in a weaker interaction with the metal and hence in a smaller charge transfer—confirmed from Bader analysis, with the exception of Mg^{2+} on Pt(111), where it is small in any case. At the same time, the effective dielectric constant increases, which we will discuss further below. Overall, the effect of the increased separation dominates and results in lower capacitances C_H.

It is somewhat surprising that there is little dependence on the metal. From the positions of the effective image planes on the three metals, we would have expected the capacitances to be ordered as Ag > Pt > Au.[33] The corresponding DFT results had been obtained for the pure surfaces; judging from Figure 1 the weakly adsorbed ions appear to shift the effective image plane, diminishing the differences between the metals. Also, the nature of the metal seems to have little to no effect on the determination of Bader charges. We would have expected the positive Bader charges to be larger on the metals with the higher work functions, which attract electrons more strongly. However, this only seems to be so in the case of Mg^{2+} on Pt.

Notably, Ca^{2+} on Pt and Mg^{2+} on Ag yield among the largest compact-layer capacitances, consistent with a shorter effective separation d_{eff} and enhanced local screening (higher ε_{eff}).

For obvious reasons C_{op} is always smaller than C_H, the differences can be traced to the partial charge transfer. C_{op} reflects the charge distribution experienced by the solvent, and hence allows us to define an effective dielectric constant.

Across our configurations, the projected metal charge density from Bader partitioning, $\sigma_{Bader} = (z\text{-}q_{ion}^{Bader})e_0/A$, varies approximately linearly with the far-field drop $\Delta\phi$ for a given metal. Extrapolating this relation to $\sigma_{Bader} = 0$ yields a composition-changing proxy for the PZC whose metal-dependent ordering aligns with the trends discussed previously. We emphasize that this proxy is a diagnostic, not a thermodynamic definition of the PZC, but it supports the idea of weak, nonspecific adsorption without pronounced nonlinear charge-transfer effects.

3.2. Effective Dielectric Constant

The effective dielectric constants are of particular interest, since it is difficult to obtain decent estimates by other means. To properly contextualize our results, we note that for pure water we can distinguish three modes for the dielectric constant with different time scales and correlation lengths:[34] the electronic response ($\epsilon_1 \approx 1.8$), an intermediate IR/librational constant ($\epsilon_2 \approx 4.9$), and the Debye (orientational) response ($\epsilon_3 \approx 78.8$), with correlation lengths on the order of ∼0.5 Å, 1 Å, and several Å, respectively.

We must also consider that we measured the distance from the conventional surface, and not from the effective image plane. Therefore, our effective values should contain a contribution from the electronic response of the metal. For the divalent cations (with six water molecules), we obtained $\epsilon_{eff} \approx 3$. Obviously, the water molecules are so firmly bound that the Debye modes do not contribute, and neither do the infrared modes, which correspond to the deformation of the water molecules. This low value seems to correspond to the electronic polarizabilities of the water and of the metal surface.

The solvation shell is less firm in the case of the monovalent ions, and the distance from the metal surface larger. Therefore, the infrared modes make a contribution, and the effective dielectric constant is higher than for the divalent. The values are close to the magical value $\epsilon \approx 6$ used in early models (e.g., Bockris−Devanathan−Müeller[35]), thereby providing physical justification for a parameter previously selected rather ad hoc. These extracted permittivities ($\epsilon_{eff} \approx 3-8$) fall within—and toward the lower half of—values reported for water nano-

https://doi.org/10.1021/acs.jpcc.5c08002
J. Phys. Chem. C XXXX, XXX, XXX−XXX

confined between insulating walls (e.g., hBN, mica, silica) which show a strongly suppressed out-of-plane response ($\epsilon_\perp \sim 2$ for few molecular layers).[36]

Because of the different correlation lengths for the three dielectric modes we expect that at distances shorter than the longest correlation length of several Å the dielectric constant increases with the separation. Figure 2 illustrates this using the

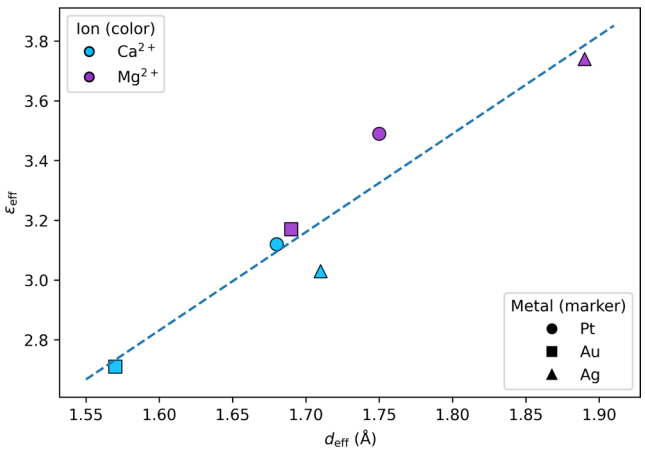

Figure 2. Effective dielectric constant ϵ_{eff} versus the binding distance d_{eff} for the six-coordinated divalent ions. The line is a guide for the eye.

six-coordinated divalent ions, which are particularly stable, as a probe. Admittedly, the range of distances is quite small, but so are the correlation lengths of the electronic and the infrared modes.

The low values of the effective dielectric constants show that the implicit solvent, with a bulk value of $\epsilon = 78.4$, does not contribute. It is largely excluded from the critical region between the ions and the metal.

We emphasize that our calculated values for the dielectric constants are not well-defined physical quantities, but they offer a convenient way to characterize the dielectric screening at the interface, which reflects the contributions of the various dielectric modes.

3.3. Electrosorption Valency

In our previous communications we had estimated the electrosorption valency of adsorbed K^+ and Ca^{2+} ions under the assumption that the adsorbed ions were supplemented by a diffuse double-layer. Here we consider the case of ideal weak adsorption, in which the excess charge on the metal electrode is exactly balanced by the adsorbed ions, so that there is no diffuse layer. This allows us to derive a simple relation for the adsorption valency γ, which is exact within this model.

We start with the relation between the dipole moment of an adsorbate and its electrosorption valency γ.

$$\mu = \frac{ze_0\epsilon_0}{C_H}\left(1 - \frac{\gamma}{z}\right) \tag{4}$$

where C_H is the Helmholtz capacitance defined above, calculated with the formal charge number z of the ions. In addition we had defined the operational capacitance C_{op} based on the real charge on the ion, which is reduced by partial charge transfer. It is related to the dipole moment through C_H. Combining the two equations results in

$$\frac{C_{op}}{C_H} = \left(1 - \frac{\gamma}{z}\right) \tag{5}$$

From the definition of the two capacitances we have

$$\frac{C_{op}}{C_H} = \frac{(z + \lambda)}{z} \tag{6}$$

where λ is the charge transferred from the metal to the ion, considered as negative in these particular cases, see Table 2.

Table 2. Electrons Transferred From Cations to Different Metal Surfaces, in Units of the Elementary Charge (Based on Bader Analysis)[a]

system	Pt	Au	Ag
$Ca^{2+} + 6H_2O$	0.40	0.37	0.39
$Ca^{2+} + 7H_2O$	0.33	0.31	0.43
$K^+ + 6H_2O$	0.04	0.04	0.04
$K^+ + 7H_2O$	0.07	0.05	0.05
$Mg^{2+} + 6H_2O$	0.01	0.25	0.27
$Mg^{2+} + 7H_2O$	0.04	0.01	0.01
$Na^+ + 6H_2O$	0.07	0.06	0.07
$Na^+ + 7H_2O$	0.07	0.07	0.06

[a]These values correspond to the electrosorption valency and are the negative of the charge transfer coefficient.

This results in $\gamma = -\lambda$, so that in our simple case the two concepts characterizing partial charge transfer differ only by the sign. Here, $\lambda < 0$ for electron transfer to the cation (reducing its positive charge); thus $C_{op} < C_H$ and $\gamma = -\lambda > 0$. This can be interpreted in terms of the Schultze–Koppitz relation[37]

$$\gamma = gz - \lambda(1 - g) \tag{7}$$

where g is the extent to which the ions penetrate the double-layer. In our case the ions form one side of the double-layer capacitor, so that they do not enter the double-layer, and hence $g = 0$.

4. CONCLUSIONS

We have investigated the double-layer formed by weakly adsorbed cations and metal electrodes. Specifically, we investigated K^+, Na^+, Ca^{2+}, Mg^{2+} adsorbed on Pt(111), Ag(111), and Au(111). There is no diffuse double-layer in our model and no special Stern layer of adsorbed water,only the hydration shell of the ions. This is realistic for the case of low electrolyte concentrations, and gives an upper limit for the capacitance when a diffuse layer is present.

Two different charge densities are useful for the interpretation: (i) the formal charge ze_0 on the ion before it is adsorbed. This is the charge that flows on adsorption in an experiment, and determines the experimental capacitance C_H. However, because of the effect of partial charge transfer the actual charge on both sides of the double-layer is smaller. We use this to define a second concept, (ii) an operational capacitance $C_{op} < C_H$, which is useful for analyzing charge and potential distribution. It is related to the dipole moment μ considered in our previous publication through: $ze_0\epsilon_0/\mu$. The potential jump due to adsorption is obtained by the change $\Delta\phi$ in the electrostatic potential at large distances. Resulting integral capacitances correspond to jumps from the PZC to an electrode potential of $-\Delta\phi$.

https://doi.org/10.1021/acs.jpcc.5c08002
J. Phys. Chem. C XXXX, XXX, XXX−XXX

The calculated capacitances C_H lie in the range ≈10−20 μFcm^{-2}, which compares well with experimental values. The two divalent cations Ca^{2+} and Mg^{2+} show a substantial partial charge transfer, which enhances their capacitance, since transferred charge contributes less to the dipole moment. In contrast, the alkali ions keep their charge. Our analysis shows that in our special case, the absence of a diffuse double-layer, the partial charge transfer differs only in sign from the electrosorption valency.

Double layer capacitances are often interpreted in terms of a parallel plate capacitor with an effective dielectric constant ϵ_{eff}. Using the adsorption distance as the effective plate separation, we have evaluated ϵ_{eff} in our systems. The adsorption distances vary in the range 1.5−5 Å so the calculated values of ϵ_{eff} correspond to averages over different distances. At short distances, only the electronic polarizabilities of the water molecules and the metal surface contribute, while at larger distances the librational modes become effective.

Within the present set of models and configurations, the effect of the metal is comparatively minor, and we do not observe a clear systematic effect on the capacitances, the charge transfer or the effective dielectric constant across Pt, Au, and Ag.

All in all, our calculations provide a compact, well-controlled reference point for discussing how weak ion adsorption, hydration, and metal response can shape the compact-layer structure and capacitance. It is important to note that these findings delineate trends under the specific conditions of our model (dilute, weakly adsorbing ions), rather than establishing universal principles.

AUTHOR INFORMATION

Corresponding Author

Fabiola Domínguez-Flores − *Institute of Theoretical Chemistry, Ulm University, 89081 Ulm, Germany;* orcid.org/0000-0002-0102-6240; Email: fabiola-1.dominguez-flores@uni-ulm.de

Authors

Axel Groß − *Institute of Theoretical Chemistry, Ulm University, 89081 Ulm, Germany;* orcid.org/0000-0003-4037-7331

Wolfgang Schmickler − *Institute of Theoretical Chemistry, Ulm University, 89081 Ulm, Germany;* orcid.org/0000-0003-4162-6010

Complete contact information is available at: https://pubs.acs.org/10.1021/acs.jpcc.5c08002

Notes

The authors declare no competing financial interest.

ACKNOWLEDGMENTS

We acknowledge support by the state of Baden-Württemberg through bwHPC, and the German Research Foundation (DFG) through grant no INST 40/575-1 FUGG (JUSTUS 2 cluster). W.S. gratefully acknowledges support by the ELSTATIK Stiftung Günter & Sylvia Lüttgens.

REFERENCES

(1) Gouy, M. Sur la constitution de la charge électrique à la surface d'un électrolyte. *J. Phys. Theor. Appl.* **1910**, *9* (1), 457−468.

(2) Chapman, D. L. LI. A contribution to the theory of electrocapillarity. *Lond. Edinb. Dubl. Phil. Mag. or Lond. Edinb. Dubl. Phil. Mag. & J. Sci.* **1913**, *25* (148), 475−481.

(3) Domínguez-Flores, F.; Melander, M. M. Electrocatalytic rate constants from dft simulations and theoretical models: Learning from each other. *Curr. Opin. Electrochem.* **2022**, *36*, 101110.

(4) Jeanmairet, G.; Rotenberg, B.; Salanne, M. Microscopic simulations of electrochemical double-layer capacitors. *Chem. Rev.* **2022**, *122* (12), 10860−10898.

(5) Woelki, S.; Köhler, H.-H.; Krienke, H. A singlet reference interaction site model theory for solid/liquid interfaces, part ii: Electrical double layers. *J. Phys. Chem. B* **2008**, *112* (11), 3365−3374.

(6) Spohr, E. Computer simulations of electrochemical interfaces. *Adv. Electrochem. Sci. Eng.* **1999**, *6*, 1−75.

(7) Domínguez-Flores, F.; Kiljunen, T.; Groß, A.; Sung, S.; Melander, M. M. Metal−water interface formation: Thermodynamics from abinitio molecular dynamics simulations. *J. Chem. Phys.* **2024**, *161* (4), 044705.

(8) Sakong, S.; Groß, A. The electric double layer at metal-water interfaces revisited based on a charge polarization scheme. *J. Chem. Phys.* **2018**, *149* (8), 084705.

(9) Schnur, S.; Groß, A. Properties of metal−water interfaces studied from first principles. *New J. Phys.* **2009**, *11* (12), 125003.

(10) Andreussi, O.; Dabo, I.; Marzari, N. Continuum models of the electrochemical diffuse layer. *J. Chem. Phys.* **2012**, *136*, 064102.

(11) Santos, E.; Schmickler, W. The inner potential in electrochemistry. *J. Solid State Electrochem.* **2024**, *28* (3−4), 1319−1322.

(12) Sundararaman, R.; Letchworth-Weaver, K.; Schwarz, K. A. Improving accuracy of electrochemical capacitance and solvation energetics in first-principles calculations. *J. Chem. Phys.* **2018**, *148* (14), 144105.

(13) Fröhlich, N. L.; Eggebeen, J. J. J.; Koper, M. T. M. Measurement of the double-layer capacitance of pt(111) in acidic conditions near the potential of zero charge. *Electrochim. Acta* **2024**, *494*, 144456.

(14) Grahame, D. C. The electrical double layer and the theory of electrocapillarity. *Chem. Rev.* **1947**, *41* (3), 441−501.

(15) Ojha, K.; Doblhoff-Dier, K.; Koper, M. T. M. Double-layer structure of the pt(111)−aqueous electrolyte interface. *Proc. Natl. Acad. Sci. U. S. A.* **2022**, *119* (3), No. e2116016119.

(16) Schmickler, W. The effect of weak adsorption on the double layer capacitance. *ChemElectroChem* **2021**, *8* (22), 4218−4222.

(17) Huang, J. Zooming into the inner helmholtz plane of pt(111)−aqueous solution interfaces: Chemisorbed water and partially charged ions. *JACS Au* **2023**, *3* (2), 550−564.

(18) Huang, J.; Domínguez-Flores, F.; Melander, M. Variants of surface charges and capacitances in electrocatalysis: Insights from density-potential functional theory embedded with an implicit chemisorption model. *PRX Energy* **2024**, *3*, 043008.

(19) Schmickler, W.; Henderson, D.; Hurwitz, H. D. Ionic adsorption at low concentrations. *Zeitschrift für Physikalische Chemie* **1988**, *160* (1−2), 191−198.

(20) Domínguez-Flores, F.; Groß, A.; Schmickler, W. Cation-induced dipole moments on single-crystal metal surfaces. *J. Phys. Chem. C* **2025**, *129* (19), 9179−9188.

(21) Kresse, G.; Furthmüller, J. Efficiency of ab-initio total energy calculations for metals and semiconductors using a plane-wave basis set. *Comput. Mater. Sci.* **1996**, *6* (1), 15−50.

(22) Kresse, G.; Furthmüller, J. Efficient iterative schemes for ab initio total-energy calculations using a plane-wave basis set. *Phys. Rev. B* **1996**, *54*, 11169−11186.

(23) Blöchl, P. E. Projector augmented-wave method. *Phys. Rev. B* **1994**, *50*, 17953−17979.

(24) Hammer, B.; Hansen, L. B.; Nørskov, J. K. Improved adsorption energetics within density-functional theory using revised perdew-burke-ernzerhof functionals. *Phys. Rev. B* **1999**, *59*, 7413−7421.

(25) Grimme, S.; Antony, J.; Ehrlich, S.; Krieg, H. A consistent and accurate ab initio parametrization of density functional dispersion

correction (DFT-D) for the 94 elements H-Pu. *J. Chem. Phys.* **2010**, *132* (15), 154104.
(26) Mathew, K.; Sundararaman, R.; Letchworth-Weaver, K.; Arias, T. A.; Hennig, R. G. Implicit solvation model for density-functional study of nanocrystal surfaces and reaction pathways. *J. Chem. Phys.* **2014**, *140* (8), 084106.
(27) Mathew, K.; Kolluru, V. S. C.; Mula, S.; Steinmann, S. N.; Hennig, R. G. Implicit self-consistent electrolyte model in plane-wave density-functional theory. *J. Chem. Phys.* **2019**, *151* (23), 234101−234112.
(28) Sotoudeh, M.; Baumgart, S.; Dillenz, M.; Döhn, J.; Forster-Tonigold, K.; Helmbrecht, K.; Stottmeister, D.; Groß, A. Ion mobility in crystalline battery materials. *Adv. Energy Mater.* **2024**, *14* (4), 2302550.
(29) Lang, N. D.; Kohn, W. Theory of metal surfaces: Induced surface charge and image potential. *Phys. Rev. B:* **1973**, *7*, 3541−3550.
(30) Grahame, D. C. Differential capacity of mercury in aqueous sodium fluoride solutions. i. effect of concentration at 25. *J. Am. Chem. Soc.* **1954**, *76* (19), 4819−4823.
(31) Hamelin, A. Trends in experimental electrochemistry on sp and sd metal single crystal electrodes. In *Trends in Interfacial Electrochemistry*; Springer: Netherlands, 1986; pp 83−102.
(32) Marcus, Y. *Ion Solvation in Neat Solvents*; Wiley, 2015; pp 107−155.
(33) Luque, N. B.; Schmickler, W. The electric double layer on graphite. *Electrochim. Acta* **2012**, *71*, 82−85.
(34) Kornyshev, A. A. *Nonlocal Electrostatics of Solvation, volume 38A of Studies in Physical and Theoretical Chemistry*; Elsevier: Amsterdam, 1985.
(35) Bockris, J. O. 'M.; Devanathan, M. A. V.; Müller, K. On the structure of charged interfaces. *Proc. Roy. Soc. Lond. Math. Phys. Sci.* **1963**, *274* (1356), 55−79.
(36) Fumagalli, L.; Esfandiar, A.; Fabregas, R.; Hu, S.; Ares, P.; Janardanan, A.; Yang, Q.; Radha, B.; Taniguchi, T.; Watanabe, K.; Gomila, G.; Novoselov, K. S.; Geim, A. K. Anomalously low dielectric constant of confined water. *Science* **2018**, *360* (6395), 1339−1342.
(37) Koppitz, F. D.; Schultze, J. W. Bond formation in electrosorbates—ii electrosorption and double layer properties in non-aqueous solvents. *Electrochim. Acta* **1976**, *21* (5), 337−343.

https://doi.org/10.1021/acs.jpcc.5c08002
J. Phys. Chem. C XXXX, XXX, XXX−XXX